Open Access

*Journal of Energy and Power Technology*

LIDSEN Publishing Inc.

Original Research

# Risks Associated with the Use of Hydrogen as an Energy Carrier or Source

Pluvinage Guy *, Capelle Julien

ENIM ENIM route d'Ars Laquenexy 57078 Metz France; E-Mails: pluvinage.guy@orange.fr; julien.capelle@enim.univ-lorraine.fr

* **Correspondence:** Pluvinage Guy; E-Mail: pluvinage.guy@orange.fr

**Academic Editor:** Brian Johnson

**Special Issue**: Hydrogen Energy: Sustainable Production, Storage and Utilisation

*Journal of Energy and Power Technology*
2022, volume 4, issue 3
doi:10.21926/jept.2203029

**Received:** March 03, 2022
**Accepted:** August 14, 2022
**Published:** September 01, 2022

**Abstract**

Hydrogen is a dangerous gas due to its low ignition energy, wide flammability range, promotion of the embrittlement of steel, and its high coefficient of permeation for polymers. The fracture toughness and failure elongation of pipe steels are strongly impacted by hydrogen embrittlement, whereas yield stress and ultimate strength are moderately impacted. Specific tools are required for the pipe defect assessment used for the transport of hydrogen, which is pure or blended with natural gas. The safety factors associated with cracks or scratches are obtained through the failure assessment diagram or the notch failure assessment diagram. The corrosion defects are assessed by limit analysis, and the estimated repair factor and dents are evaluated by computing the damage value under service pressure. The design factor in the calculation of the maximum admissible operating pressure (MAOP) is modified depending on the location of the pipes to account for the lethal risks from the torch effect or explosion. It is crucial to monitor the leaks due to hydrogen permeation through domestic hydrogen distribution networks, particularly in closed areas.

**Keywords**

Hydrogen; risks; embrittlement; lethal effects; permeation

## 1. Introduction

To protect the environment, the dependence on non-renewable sources of energy such as oil and coal hydrogen must be reduced. In the foreseeable future, hydrogen is a candidate as a substantial element in the energy distribution if it can be produced from green sources.

In addition to being a sustainable energy carrier, hydrogen is considered a source of energy. Since electricity produced by renewable energies such as solar and wind cannot be stored, conversion into hydrogen is a way to store energy. Hydrogen can be transported as gas, liquid, or solid. One of the major uses of hydrogen is as fuel in electric fuel cell vehicles (EFCV). Furthermore, hydrogen can be used as an energy source in stationary cell systems for domestic uses and emergency distribution.

According to the power to gas (P2G) concept, hydrogen is produced at home from green electricity using a domestic electrolyzer. The hydrogen that is transported is mainly blended with natural gas. The risks associated with hydrogen can be technical, social, environmental, or lethal, which necessitates the planning of a specific risk policy. Moreover, hydrogen is transported by pipelines rather than by trucks on the road for safety concerns.

The limiting factor in the transport of hydrogen by trucks is volume. To obtain the energy equivalent of a petrol tank truck, 22 trucks of hydrogen at 200 bars or 3 liquefied hydrogen tank trucks (a 40-ton truck transports a maximum of 3.5 t of liquid H2) are required. The amount of energy expended for the transportation of gaseous and liquid hydrogen per truck is very high (respectively 80% and 11% of the energy content delivered to 600 km). It must be emphasized that security issues exist in the actual scenario.

We distinguish between the transport of hydrogen (pure or blended) in large pipes made of steel at a high service pressure (generally 6.9 MPa) and the distribution for domestic application in polymer (PE) pipes at low pressure (0.39 MPa).

The durability of metallic pipes is impacted by prolonged exposure to hydrogen. This is the case of pipes working at high service pressures with high concentrations of hydrogen. This phenomenon is called hydrogen embrittlement (HE). When the hydrogen concentration overcomes a threshold, a decrease in the mechanical properties of the steel is observed.

The domestic distribution is ensured by polyethylene (PE) pipe. However, the permeation coefficient of high-density PE (HDPE) is high. At a service pressure of 4 bar and a mixture of 90% CH4 + 10%$H^2$, the volume of hydrogen passing through the wall is estimated at 546 l/km/year [1]. For indoor installation in sensitive locations, it is necessary to control the continuous hydrogen flow through polymer pipe walls with a local sensor for security.

In this paper, the following major risks induced by the use of hydrogen are presented:

- pipe failures resulting from defects due to hydrogen embrittlement.
- lethal damage due to heat or explosion overpressure after hydrogen ignition.
- explosion due to hydrogen permeation.

To investigate these three kinds of risks (failure, lethal risks due to explosion and torch effects, and hydrogen accumulation due to permeation), the following fundamental concepts are considered:

- defect assessment following hydrogen embrittlement using a failure assessment Diagram (FAD) or a notch failure assessment diagram (NFAD), limit analysis (LA), and strain-based design (SBD).
- lethal heat radiation risks arising as a consequence of the intensity of the heat flux and the duration of exposure. The overpressure was due to the explosion.
- lethal explosion risks based on the equivalent mass of TNT and the resulting overpressure due to the explosion.
- the gas loss calculated from the permeation coefficient of hydrogen.

The results presented in Sections 3 and 4 summarize the prior works of the author along with the references. The results extracted from the EU NATURALHY contract are presented in Section 5. Although the authors were involved in other projects, they all contributed to this contract.

## 2. Hydrogen Properties as a Molecule in Gases and an Atom in Metallic Solids

Hydrogen has a relatively low molecular weight of 2.01594 g/mol. Its density is 0.071 g/L at 0°C and 1 atmosphere as a gas. Its relative density is 0.0695 when compared to air.

Hydrogen is highly flammable and has an "NFPA" rate of 4 [1]. It is flammable after ignition when mixed with 4% of air. Table 1 lists the physical characteristics of hydrogen.

**Table 1** Physical characteristics of hydrogen.

| | | | |
|---|---|---|---|
| Molecular weight | 2.016 g/mol | NFPA ratings | 4 |
| Boiling point at atmospheric atmosphere | -252.8°C | Flammable limits in air | 4–75% |
| Density of gas at boiling point | 67.76 Kg/$m^3$ | Auto-ignition temperature | 400°C |
| Melting point | -259.2°C | Combustion speed | 3.5 m/s |
| Latent heat of vaporization at boiling | 446.0 KJ/Kg | Ignition minimum energy | 0.02 mJ |
| Specific gravity at 1 atm | 0.696 | Explosion energy | 2.02 Kg TNT/g |

The history of the Zeppelin Hindenburg serves as an example of the low ignition energy of hydrogen. On May 6, 1937, this rigid-hulled airship burst into flames on arrival at Lakehurst airport, near New York. Upon touching the mooring mast, her hull caught fire, probably due to static electricity (Figure 1).

**Figure 1** Zeppelin Hindenburg accident (May 6th, 1937).

Hydrogen has the lowest ignition energy (hydrogen 0.02 mJ, natural gas 0.29 mJ, propane 0.26 mJ, and gasoline vapor 0.24 mJ) when compared to other fuel gases. It has a wide flammability range (4–75%), which is less than acetylene and ethylene oxide. The absorption of hydrogen by steel results in embrittlement and probable failures in pipes.

Structural defects are always present in solid materials. Metallic imperfections such as gaps, dislocations, grain boundaries, pores, and inclusions serve as trapping sites for hydrogen. Alloying elements form hydrides with carbon and sulfur, which can act as trapping sites. They interact with hydrogen to form gases such as CH4 and H2S, which generate blisters in the material. The transport rate of hydrogen through the material is decreased by hydrogen trapping. Therefore, in these trapping sites, further diffusion of hydrogen becomes difficult. The residence time at these sites increases more than that at a normal distribution in the network. In a metallic system, hydrogen transport can become extremely complex.

According to [2], the different types of trapping were established and classified depending on the following:

- the location of the trapping (trapping in volume or on the surface).
- its origin (electronic, chemical, or elastic interactions).
- the existence of long-range interaction between the trap and the interstitial atom (“attractive,” “physical” or “mixed” traps).
- the value of the hydrogen-trap interaction energy: At a given temperature, “irreversible” traps, i.e., the sites at the level where the probability of de-trapping is almost zero, are characterized by high interaction energy. For a "reversible" trap of lower energy, there is a balance between the hydrogen atoms which occupy the trap and the sites of the network (the idea of a "reversible" or "irreversible" trap makes sense only for a given temperature) [3].
- the size of the trap, which can be specific (interstitial atom, vacancy), linear (dislocation), plane (interface between phases, grain boundary), or volumetric (microporosity, crack).

Several mechanisms are used to explain hydrogen embrittlement, which include the following:

- weakening of metal-metal atomic bonds [4],
- modification of plasticity,
- decohesion/dislocation emission competition [5],
- molecular recombination in defects,

- triaxiality of stresses.

At the tip of the crack, a high concentration of hydrogen is localized, which is sufficient to initiate cleavage failure. Therefore, this model is particularly interesting for CC metals, which can cleave very easily (the ductile and brittle transition temperatures are near to ambient). Furthermore, it is plausible that the absorption of hydrogen enables a transition from a ductile fracture behavior to brittle behavior.

According to this mechanism, interstitial hydrogen determines the embrittlement of a material when it is subjected to mechanical stresses. It is based on the increase in the local concentration of hydrogen in stress fields with high triaxiality like crack tips, as well as on the weakening of the metal-metal bonds by modifying the electronic environment of the atoms. Due to the high local concentration of hydrogen, the effect is more pronounced. The main parameter is the intensity of the elastic stress field, which depends on the mechanical stress and the microstructure of the material. The embrittlement and the delayed fracture of high-strength steels are usually explained by this mechanism. The embrittlement mechanism is associated with transport by dislocations and pinning by traps. The moving dislocations accelerate the transport of hydrogen. Hydrogen is accumulated on defects by mobile dislocations under specific conditions. These defects act as obstacles to the movement of dislocations. Dislocation stacks generate high stresses, which promote crack initiation and propagation. Local hydrogen accumulation is favored by the coplanar motion of dislocations. The nature and distribution of defects in the microstructure restrict the movement of dislocations.

The effect of supersaturation associated with the sudden change in temperature in a material containing a high quantity of hydrogen in the absence of imposed stress causes blistering and internal cracking. The recombination of defects results in microcavities where the hydrogen pressure is high enough to form blisters. This defect is typically seen in pipes transporting hydrogen [6].

A brittle metal hydride that facilitates brittle failure is obtained ahead of a crack tip in a region of high triaxiality. Brittle phase cracking can lead to crack propagation.

## 3. Ductile-Brittle Transition Due to Hydrogen Embrittlement

Fracture resistance is impacted by hydrogen embrittlement, among other reductions in mechanical properties. This is observed following the 3-point bending test on notched specimens. Electrolysis is used to subject the specimens made of pipe steel to hydrogenation for a long period. Subsequently, they are loaded at a slow strain rate until fracture. Figure 2 shows the load-displacement diagram that was recorded during the test. To detect fracture initiation, the acoustic emission method [7] is utilized. The area under the load-displacement curves up to the load at initiation is defined as the critical energy or initiation energy $U_i$ or fracture toughness.

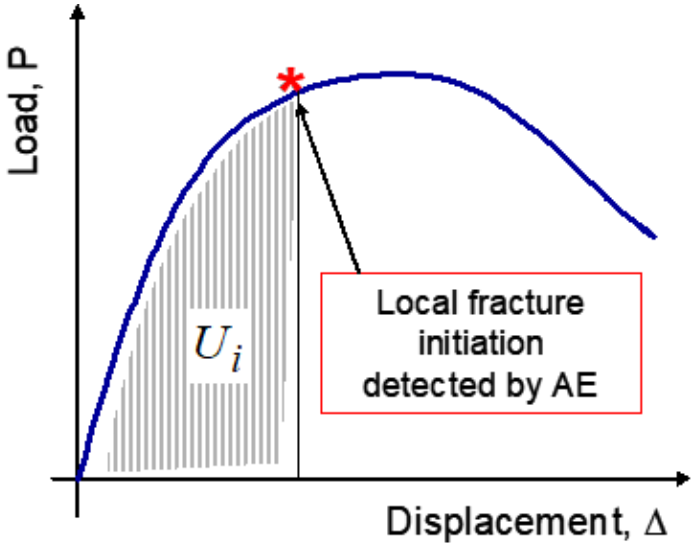


**Figure 2** Energy initiation defined on a load-displacement curve [7].

As the concentration of hydrogen increases, the fracture resistance drops sharply. The critical hydrogen concentration can be determined as per the procedure described in Figure 3 owing to the drop in fracture resistance. As shown in Table 2 for 3 steel pipes, the critical hydrogen concentration $C_H^*$ decreases with the yield stress [7].

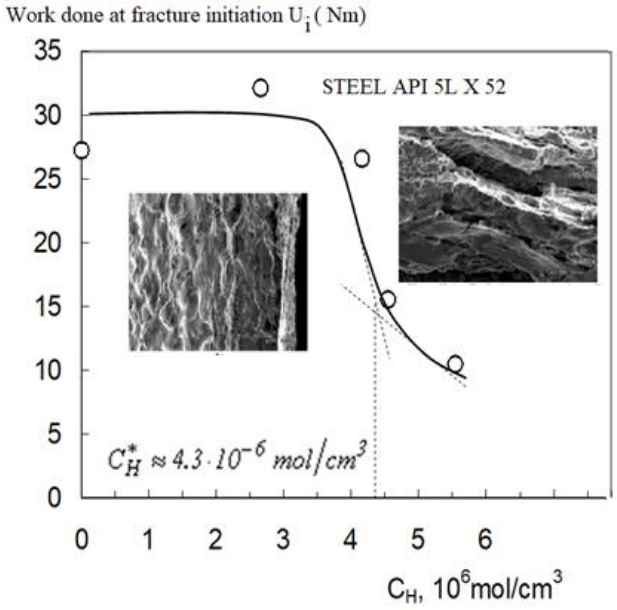


**Figure 3** Critical hydrogen concentration of API X52 determined from work done at fracture initiation [7].

**Table 2** Critical hydrogen concentrations $C_H^*$ for three pipeline steels [7].

| Steel | Yield stress (MPa) | $C_H^*$, $10^6$ mol/cm$^3$ |
|---|---|---|
| X52 | 410 | 4.3 |
| X70 | 590 | 2.3 |
| X100 | 866 | 1.5 |

The critical hydrogen concentration is fitted by a power function versus the yield stress $\sigma_y$ or the ultimate stress $\sigma_{ul}$.

$$C_H^* = B_1.\left(\sigma_y\right)^{n_1} \quad (1)$$

$$C_H^* = B_2.(\sigma_{ul})^{n_2} \quad (2)$$

where $B_1, B_2, n_1, n_2$ are material constants and depend on the test conditions. The basic strategy to prevent the risk of brittle fracture in steel pipes is to prevent cleavage by maintaining sufficient ductility. Several codes at Level 1 provide the rules to satisfy this condition, including API 579–1 ASME FFS-1 [8] for pipes in general and ASMEB31.12–2019 hydrogen piping and pipelines [9] for pipes used for hydrogen transport.

The operating or service temperature $T_s$ or the minimum allowable temperature (MAT) must be higher than the brittle-ductile transition temperature (DBTT) $T_t$.

$$T_S \; or \; MAT > T_t \quad (3)$$

The operating temperature $T_s$ and the ambient temperature are different. $T_s$ depends on the choice or obligation of the code. Transition temperatures depend on failure tests such as Charpy tests or drop weight tearing tests (DWTT) and specimen geometries such as standard Charpy specimens, mini-Charpy specimens, or sub-sized Charpy specimens. A test with similar constraints yields a value close to the "structure or component" transition temperature, $T_{comp}$. This determines the design degree of conservatism of this approach. Since the transition temperature is sensitive to constraints, it falls as the occurrence of plastic deformation decreases [10].

According to ASMEB31.12–2019 hydrogen piping and pipelines, "all impact tests shall be made using standard 10 mm square cross-section Charpy V specimens bars except when the material shape or thickness does not permit"[9]. The Charpy energy $K_{cv}$ (J) versus temperature curve is fitted as given in Eq.(4) [11].

$$\mathrm{K_{cv}}(J) = \mathrm{A_{cv}} + \mathrm{B_{cv}}\tanh\left[\frac{(\mathrm{T} - \mathrm{D_{cv}})}{\mathrm{C_{cv}}}\right] \quad (4)$$

where $A_{CV}$, $B_{CV}$, $C_{CV}$, and $D_{CV}$ are constants. $A_{CV}$ represents the Charpy energy at the transition temperature, $B_{CV}$ is the energy jump between the brittle and ductile plateaus, and $C_{CV}$ represents the temperature range of the Charpy energy transition. $D_{CV}$ represents the brittle-ductile transition temperature. Constants $\mathrm{A_{CV}}$, $\mathrm{B_{CV}}$, $\mathrm{C_{CV}}$, and $\mathrm{D_{CV}}$ are related to the upper shelf energy (USE), the lower shelf energy (LSE), and DBTT as:

$$\mathrm{A_{CV}} + \mathrm{B_{CV}} = USE$$

$$\mathrm{A_{CV}} - \mathrm{B_{CV}} = LES$$

$$\mathrm{D_{CV}} = DBTT \quad (5)$$

The impact of hydrogen embrittlement on DBTT was examined [12] using the ½ mini-Charpy and standard Charpy specimen types.

Figure 4 and Figure 5 compare the Charpy energy versus temperature curves with and without hydrogen embrittlement for the two types of specimens made in X65 steel. Figure 4 displays the Charpy energy curve versus temperature for the ½ mini-Charpy with and without HE. Figure 5 is related to standard Charpy specimens. The curves are fitted according to equation 8. Table 3 present the constants $A_{CV}$, $B_{CV}$, $C_{CV}$, and $D_{CV}$ of Eq. (4).

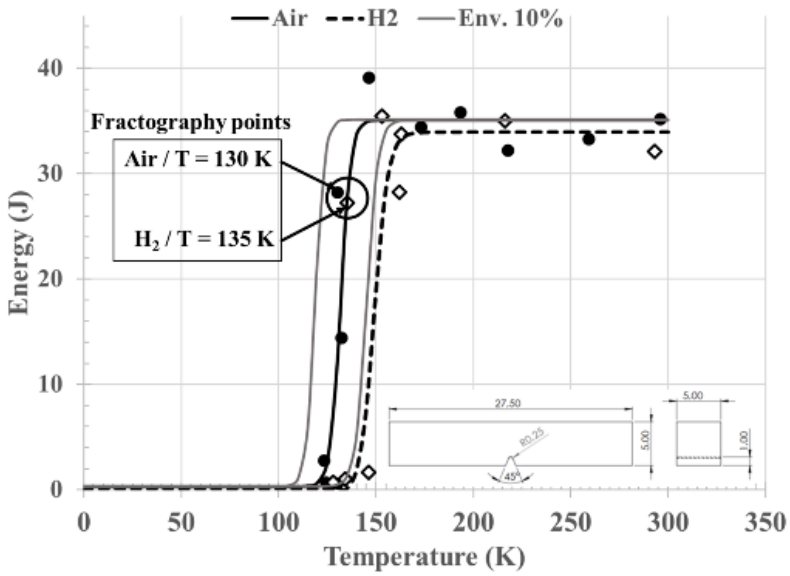


**Figure 4** Curves of Charpy energy versus temperature for ½ mini-Charpy with and without HE, pipe steel X65 [12].

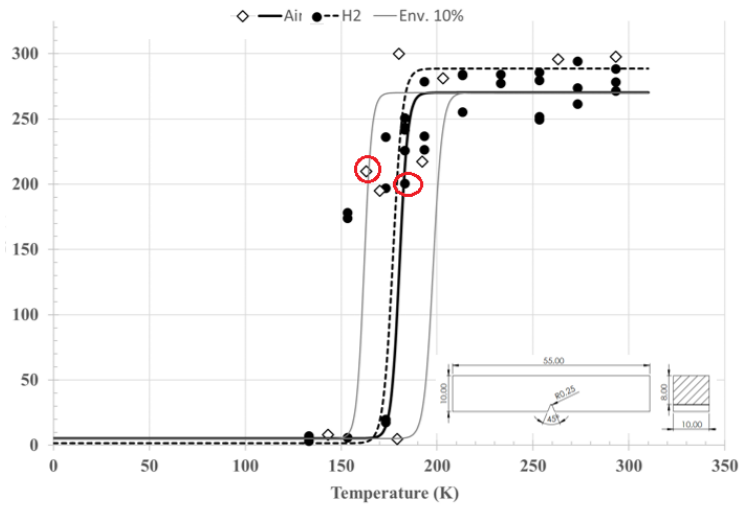


**Figure 5** Curves of Charpy energy versus temperature for Standard-Charpy with and without HE, steel X65[12].

**Table 3** Parameters ACV, BCV, CCV, and DCV for ½ mini-Charpy specimens with and without HE.

| | $A_{CV}$ (J) | $B_{CV}$ (J) | $C_{CV}$ (K) | $D_{CV}$ (K) |
|---|---|---|---|---|

| | | | | |
|---|---|---|---|---|
| Standard without HE | 137.7 | 132.4 | 4.3 | 180 |
| Standard with HE | 145 | 143.5 | 5 | 177 |
| Half-Charpy with HE | 16.7 | 17.3 | 7.1 | 149 |
| Half-Charpy without HE | 17.7 | 17.4 | 5.17 | 132 |

A slight increase in DBTT is observed, which is 17 K for the ½ mini-Charpy transition temperature and 3 K for the standard Charpy specimen. A thickness effect on the shift of DBTT is inferred after HE. This small shift must be compared with the natural scatter of the Charpy impact test. Although an estimated scatter band of the Charpy energy-temperature curve is made, the real scatter band with many tests is not available. The coefficient of variation (COV) of the yield stress of the API 5L X65 steel is 5.25% [13]. Based on this result, the upper and lower bound of COV for $C_{CV}$ and $D_{CV}$ were fixed at 10%.

Figure 5 and Figure 6 illustrate the associated scatter bands. The DBTT shift is greater for ½ mini-Charpy specimens than the width of the scatter band. Therefore, DBTT is affected by HE.

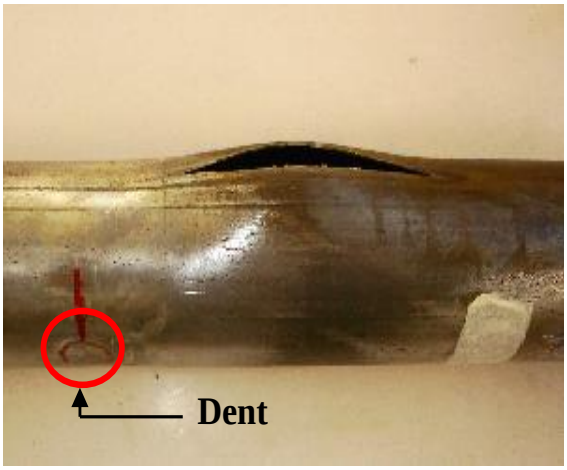


**Figure 6** Example of pipe failure emanating from the dent.

## 4. Pipe Failure Risks in the Transport of Pure or Blended Hydrogen

For safety and economic reasons, liquid or gas is transported to the market area for consumption through pipelines. In 120 countries around the world, there is approximately 3,500,000 km of pipeline (2014). Three countries, the United States (65%), Russia (8%), and Canada (3%) accounted for 75% of all pipelines.

Compared to rails and trucks, the transport of crude oil via pipeline causes fewer fatalities and property damage. Moreover, the spilling of oil is less in pipelines than in trucks. The safety and reliability of pipelines depend on the mechanical damage caused by fabrication or external interferences, as well as the deterioration of the pipeline metal over time and welded joints. The other causes of damage include human errors or vandalism.

Table 4 presents the different causes of incidents with their respective percentage of occurrence [14]. In Europe, external interference is the major cause of service failures. As shown in Figure 6, the main types of damage are gouges and dents. A defect assessment in a pipeline is conducted using specific tools depending on the types of defects and fracture modes.

**Table 4** Causes and percentage of incidents in gas pipes [14].

| External Interference | Construction defect/ material failure | Corrosion | Ground Movement | Hot-Tap made by Error | Other and Unknown |
|---|---|---|---|---|---|
| 49.6% | 16.5% | 15.3% | 7.3% | 4.6% | 6.7% |

### *4.1 The Influence of Hydrogen Embrittlement on the Harmfulness of Pipe Cracks*

The highest severity is observed in cracks. Generally, all defects are categorized as cracks in codes, which is a conservative approach. Long pipes have real cracks because they are assembled by welding. As shown in Figure 7, cracks are detected in welds or heat-affected zones, and they are often associated with porosities and slag inclusions.

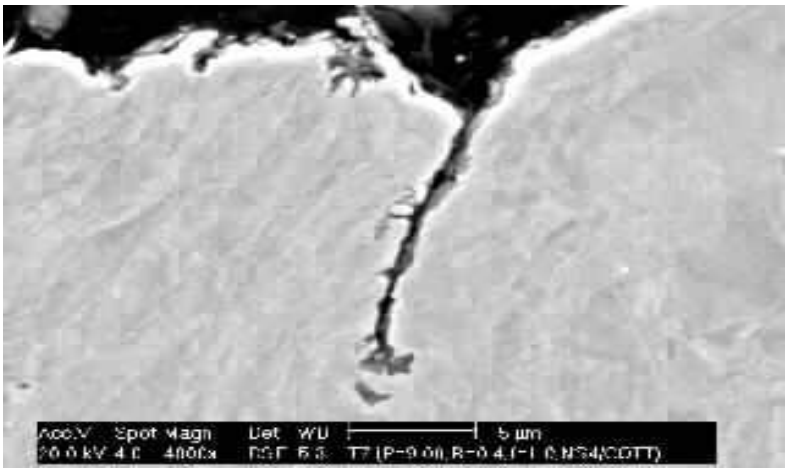


**Figure 7** Crack in a pipe welded joint.

The irregular shape of a crack for internal cracks and surface is described as flat elliptical and semi-elliptical, respectively. The dimensions of the elliptical or semi-elliptical crack are obtained by enclosing the irregular shape in a rectangle of length 2c and width 2a for internal cracks and length 2c and depth a for surface cracks. The crack driving force is determined by computing the applied stress intensity factor using an analytical solution or the finite element method. The admissibility of a crack in the pipe is determined by comparing the safety factor $f_s$ with a prescribed value of $f_s = 2$. This safety factor is provided by the failure assessment diagram (FAD).

The FAD is a plane representation of the fracture criterion associated with the critical stress intensity factor. Figure 8 shows the typical representation of a FAD. The non-dimensional crack driving force and non-dimensional applied stress are employed as coordinates for all materials and applications. The applied non-dimensional crack driving force is defined as the ratio of the applied stress intensity factor $K_{ap}$ to the fracture toughness of the material $K_{Ic}$ :

$$k_r^* = {K_{ap}}\Big/{K_{Ic}} \tag{6}$$

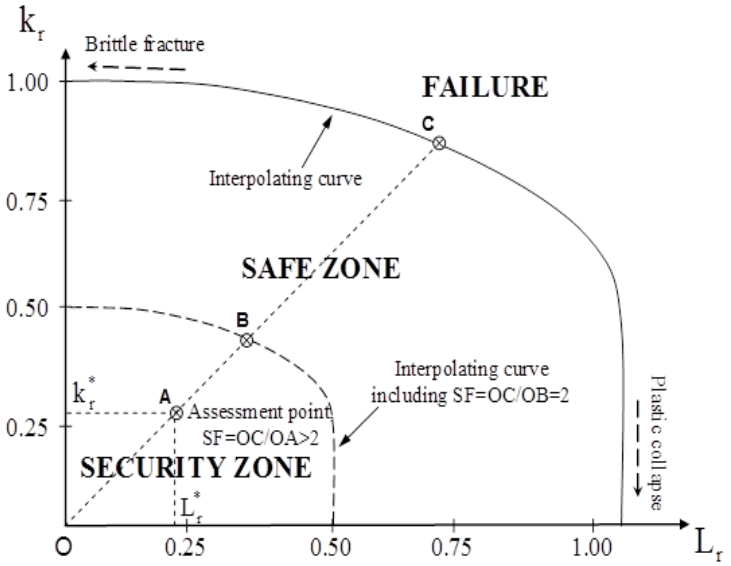


**Figure 8** Typical presentation of Failure Assessment Diagram (FAD) [15].

Furthermore, the *J* integral or the crack opening displacement is used to define the non-dimensional crack driving force as:

$$k_r^* = \sqrt{J_{ap}/J_{mat}} \; or \; k_r = \sqrt{\delta_{ap}/\delta_{mat}} \tag{7}$$

where $J_{ap}$, $\delta_{ap}$ are the applied *J* integral and crack opening displacement, respectively. The fracture toughness of the material, expressed as $J_{mat}$ or $\delta_{mat}$, is the critical value of *J* integral or crack opening displacement.

The non-dimensional stress is the ratio of the gross stress to flow stress (is. The flow stress is chosen as the yield stress $\sigma_Y$, the ultimate stress $\sigma_{ul}$, or the classic flow stress $\sigma_0 = \frac{(\sigma_y+\sigma_{ul})}{2}$.

Failure conditions are represented by an assessment point in the FAD with coordinates $L_r^*, k_r^*$. The critical curve (or failure curve) is given by $k_{r,c} = f(L_{r,c})$. Figure 9 is obtained from the coordinates $[L_{r,c}, k_{r,c}]$.

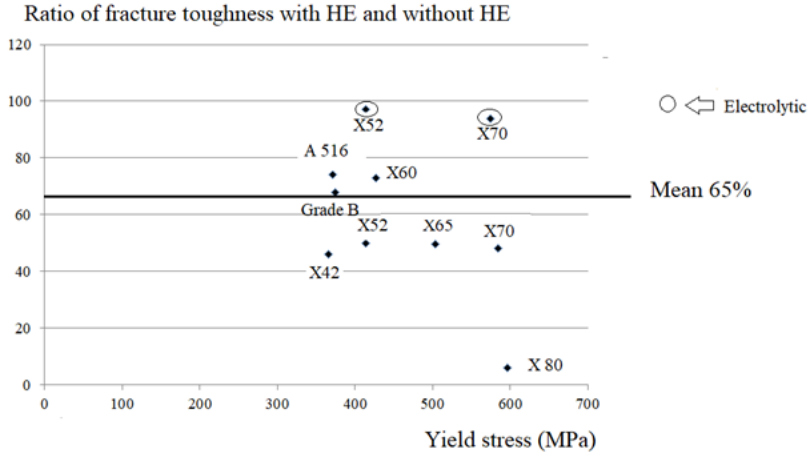


**Figure 9** The ratio of fracture toughness with and without HE for 10 steel pipes [16].

When the load increases from 0 to the critical load $P_c$, the loading path OC associated with a defect and service conditions becomes linear. The coordinates at assessment point B are $L_r^*$ and $k_r^*$. No failure occurs if this assessment point is inside the safe zone. Critical conditions are reached if the assessment point is on the assessment curves or above. The associated safety factor is expressed by the following relationship:

$$f_s = \frac{OC}{OA} \tag{8}$$

OA and OC are segments from the origin O to the assessment point B and the intercept failure curve C. This relation is a consequence of the $L_r$ and $k_r$ definitions, which are both proportional to the gross stress. The criticality of the situation is determined by comparing the obtained safety factor to the conventional value of $f_s = 2$.

After hydrogen embrittlement (HE), the mechanical properties of 10 pipe steels were examined based on the data extracted from the literature.

Data were collected under the same hydrogen gas pressure (6.9 MPa H2). Table 5 reports the values of yield stress $\sigma_y$, ultimate strength $\sigma_{ul}$, and fracture toughness $K_{Ic}$. The fracture toughness decreases by 33% in the yield stress range [350–600 MPa] as mean values (Figure 9). The fracture toughness of the pipe steel decreases with an increase in hydrogen pressure and a decrease in electrolytic potential.

**Table 5** Mechanical characteristics of pipe steels after hydrogen embrittlement under gas pressure.

| Steel | $\sigma_y$ (MPa) | $\sigma_{ul}$ (MPa) | $K_c$ (MPa√m) |
|---|---|---|---|
| 1080 | 414 | 784 | 111 |
| A 516 | 364 | 551 | 102 |
| API 5L Grade B | 299 | 518 | 89 |
| API5L X 42 | 331 | 490 | 69 |
| API5L X 46 | 374 | | |
| API5L X 52 | 429 | 597 | 108 |
| API 5L X 60 | 422 | 590 | 142 |
| API 5L X 65 | 506 | 611 | 180 |
| API 5L X 70 | 566 | 653 | 197 |
| API 5L X 80 | 566 | 707 | 56 |

The non-dimensional crack driving force $k_r$ decreases with HE due to the reduction in fracture toughness. Since HE has a negligible effect on flow stress, the non-dimensional load is minimally impacted. The loading path under HE is above the loading path for conditions without HE (Figure 10). Therefore, the safety factor is modified.

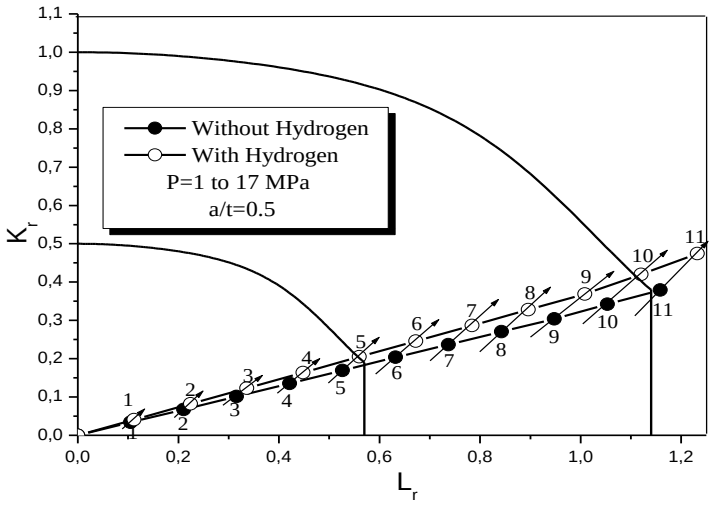


**Figure 10** Loading paths with and without HE. Pipe diameter D = 611 mm and thickness t = 11 mm, relative defect depth a/t/0.5, API 5L X52 steel [17].

Figure 10 depicts a pipe (diameter is D = 611 mm and thickness t = 11 mm) made from API 5L X52 steel and subjected to internal pressure. The pipe defect is considered as an internal semi-elliptical with a thickness ratio a/t = 0.5 and an aspect ratio a/c = 0.5.

### *4.2 The Influence of Hydrogen Embrittlement on the Harmfulness of Pipe Gouges*

The major cause of service failures in Europe is external interference. These damages can be classified into gouges and dents. Typically, gouges are caused by scrapers or agricultural devices. Figure 11 presents an example of several gouges made by a scraper.


**Figure 11** Gouges on the pipe surface.

To assess external interferences, different tools are used depending on the defect types and fracture modes. The classical fracture toughness $K_{Ic}$ is determined from cracked specimens and plane strain conditions. The use of pre-cracked specimens is both time-consuming and expensive. Due to sensitivity to crack propagation, it is impossible to pre-crack brittle specimens like ceramics. Therefore, using notched specimens is more advantageous, and cheaper. In general, the notch fracture toughness $K_{\rho,c}$ measured with notched specimens is higher than that measured with a cracked specimen. The failure emanating from a notch is treated as a local fracture criterion in notch fracture mechanics (NFM)[15]. The volume fracture process (VFP) is considered in the

volumetric method [15]. The diameter of the cylindrical shape in VFP corresponds to the “effective distance”. VFP is the "highly stressed volume", which contains the required strain energy for fracture. Because the effective distance is not a material constant and is dependent on the loading mode, geometry of the structure, and load level, its magnitude is a matter of debate. The distribution of the opening stresses yields the effective distance $X_{ef}$. Figure 12 presents the elastic-plastic stress distribution along the ligament and can be divided into several zones. A thorough examination of the fracture initiation sites proves that the effective distance corresponds to the beginning of zone III. The relative stress gradient (χ) of the opening stress $\sigma_{yy}$ distribution is expressed by Eq. 9:

$$\chi(\mathrm{r}) = \frac{1}{\sigma_{\mathrm{yy(r)}}} . \frac{\partial \sigma_{\mathrm{yy(r)}}}{\partial \mathrm{r}} \tag{9}$$

The effective distance is associated with the minimum of χ. Effective stress $\sigma_{ef}$ is defined as the average value of $\sigma_{yy}$ over $X_{ef}$.

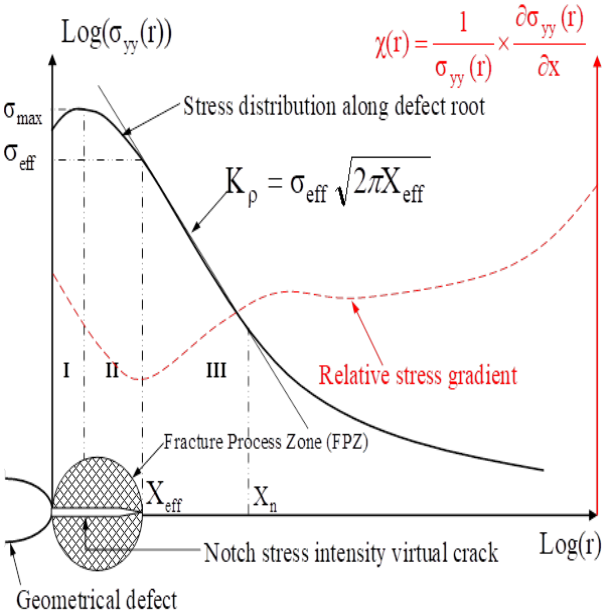


**Figure 12** Distribution of opening stresses along a ligament ahead of a blunt defect. Determination of effective distance [15].

The opening stress is multiplied by a weight function to consider the effect of the geometry, the loading mode, and the action distance r. The effective stress is given by:

$$\sigma_{ef} = \frac{1}{X_{ef}} . \int_0^{X_{ef}} \sigma_{yy}(r) . \Phi(r) . dr \tag{10}$$

Figure 12 describes the method for determining the effective distance using the relative stress gradient. Further information on Eqs. 9 and 10 is given in [15].

The notch stress intensity factor (NSIF) $K_\rho$ is a function of the effective distance $X_{ef}$ and stress $\sigma_{ef}$

$$K_\rho = \sigma_{ef} \left(2\pi X_{ef}\right)^{\alpha} \tag{11}$$

α is the slope of the stress distribution in region III. The fracture criterion is given by:

$$K_{\rho} = K_{\rho,c} \tag{12}$$

$K_{\rho,c}$ is the notch fracture toughness of the material. The notch fracture toughness is a linear function of the square root of the notch radius. It is a constant and equal to $K_{Ic}$ below a critical value $\rho_c$ [18]. For steel, $\rho_c$ is of the order of a few tenths of a millimeter.

$$K_{\rho,c} = K_{I,c} \text{ pour} \rho \leq \rho_c$$

$$K_{\rho,c} = K_{I,c} + A.\sqrt{\rho} \text{ for } \rho > \rho_c \tag{13}$$

The additional contribution A. √ρ is provided by the plastic work in the notch plastic zone.

When the defect is to be assessed by the FAD method, it is necessary to modify Eq. 6 and replace the fracture toughness $K_{IC}$ by $K_{\rho,c}$ due to the sensitivity of the fracture toughness with notch radius.

$$k_r = \frac{K_{\rho}}{K_{\rho,c}} \tag{14}$$

where $K_{\rho}$ is the applied notch stress intensity factor.

The $L_r$ parameter is the same for a notch or a crack and the failure assessment diagram. The notch failure assessment diagram (NFAD), which is used to assess notch-like defects with a non-zero radius, is formed by substituting Eq. 14 for Eq. 6.

The impact of hydrogen on the safety factor associated with a semi-elliptical notch type surface defect (a/c = 0.2; a/t = 0.5) in an API 5L X52 steel pipe was analyzed [19].

The pipe has a thickness of 6.1 mm, a diameter of 219.1 mm, and an operating pressure of 70 bars. Table 6 presents the coordinates of the assessment points.

**Table 6** Data related to Figure 12.

| | $K_{\rho,app}$ (MPa√m) | $K_{\rho,c}$ (MPa√m) | $\sigma_{\theta\theta}$ (MPa) | $R_e$ (MPa) | $R_m$ (MPa) | $\sigma_0$ (MPa) | ($l_r$; $k_{,r}$) | Safety factor |
|---|---|---|---|---|---|---|---|---|
| Natural gas | 14, 6 | 57, 21 | 125, 7 | 431 | 526 | 478, 5 | (0, 26; 0, 25) | 3, 06 |
| Hydrogen | 14, 6 | 41, 78 | 125, 7 | 450 | 547 | 498, 5 | (0, 25; 0, 35) | 2, 54 |

Table 6 and Figure 13 summarize the impact of hydrogen on the safety and security factors. Although the safety factor is reduced by about 20% due to hydrogen, it remains greater than 2. Therefore, the assessment points are in the security zone.

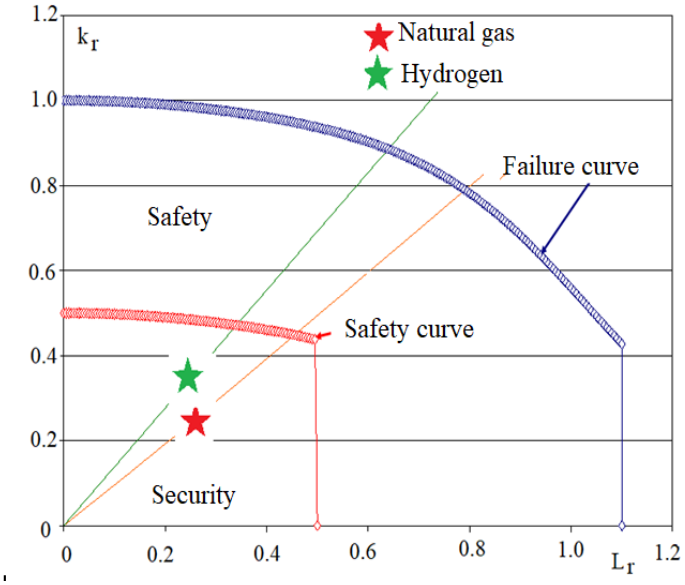


**Figure 13** Assessment points under natural gas and hydrogen pressure for a semi-elliptical surface defect (a/c = 0.2; a/t = 0.5)[19].

### *4.3 The Influence of Hydrogen Embrittlement on the Harmfulness of Pipe Dents*

A dent in a pipeline is a permanent plastic deformation of the circular cross-section of the pipe (Figure 13). The geometry of the dent causes local stress and strain concentration and a local reduction in the pipe diameter. The dent depth is defined as the maximum reduction in the diameter of the pipe. The different types of dents include smooth dents, kinked dents, plain dents, unconstrained dents, and constrained dents (Figure 14).


**Figure 14** Plain dent in a pipe.

The failure elongation of the pipe steels decreases strongly under the influence of HE (Figure 15). The δ ratio is defined as (δ = A% ($H^2$)/A% (air)); δ versus yield stress of the pipe steel is a decreasing function [20]:

$$\delta = -0.009\sigma_y + 1.29 \quad (15)$$

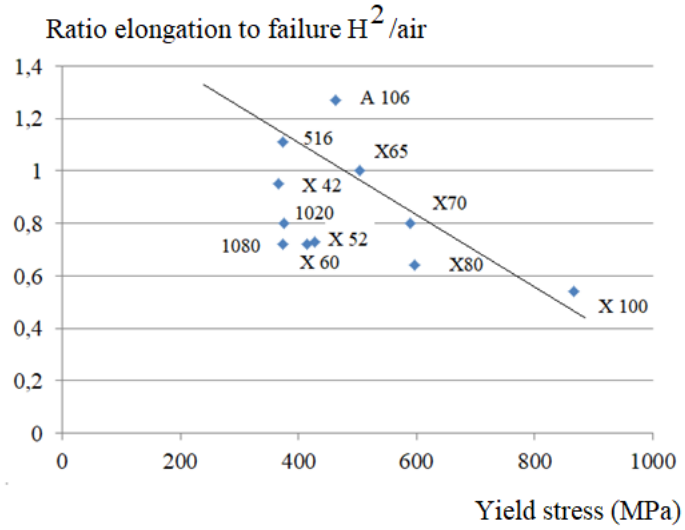


**Figure 15** Evolution of the ratio elongation to failure after HE and elongation to failure without HE versus yield stress of pipe steel [16].

Dents can be assessed using the strain-based design (SBD), which is based on failure elongation. The most recent SBD is made according to a local strain criterion in which the failure criterion is satisfied when the maximum local strain $\varepsilon_{l,c}$ is equal to the corrected failure strain $\varepsilon_{f,c}$.

$$\varepsilon_{l,c} = \varepsilon_f \tag{16}$$

The corrected failure strain accounts for both the hydrostatic pressure $\sigma_m$ and the Lode angle $\theta_L$.

$$\varepsilon_f(\sigma_m, \theta_L) = \epsilon_{f,0} * \mu_{\sigma_m}(\sigma_m) * \mu_{\theta_L}(\theta_L) \tag{17}$$

$\mu_{\sigma_m}(\sigma_m)\ and\ \mu_{\theta_L}(\theta_L)$ are dependent on the hydrostatic pressure and the Lode angle, $\epsilon_{f,0}$ is the reference or material failure strain. The damage criterion developed by Oyane et al. [21] is integrated with this failure criterion and is given by,

$$\mathrm{D} = \frac{1}{\mathrm{C}_2}\int_0^{\bar{\varepsilon}_\mathrm{f}} \left(\mathrm{C}_1 + \frac{\sigma_\mathrm{h}}{\bar{\sigma}}\right) \mathrm{d}\bar{\varepsilon} \tag{18}$$

During failure, damage D = $D_c$, where $D_c$ is the critical damage. $\bar{\varepsilon_f}$ denotes the equivalent failure strain, $\sigma_m$ denotes the hydrostatic stress, $\bar{\sigma}$ denotes the equivalent stress; $\bar{\varepsilon}$ denotes the equivalent strain; $C_1$ and $C_2$ are material constants and $C_2$ is identical to $\varepsilon_{f,0} = C_2$.

This criterion has been used to assess various dent depths. As shown in Figure 15, for a pipe made in API 5L X52 steel (failure elongation is 31.5%, which is 23% after HE), the visible dent is considered. Due to the reduced failure elongation, HE causes greater critical damage. The maximum damage once HE is attained for the given ratio is shown in Figure 16, where $H_0$ is the dent depth, and $D_e$ is the external diameter of the pipe made of steel API5L X52, having a diameter of 89 mm and a thickness of 3.2 mm.

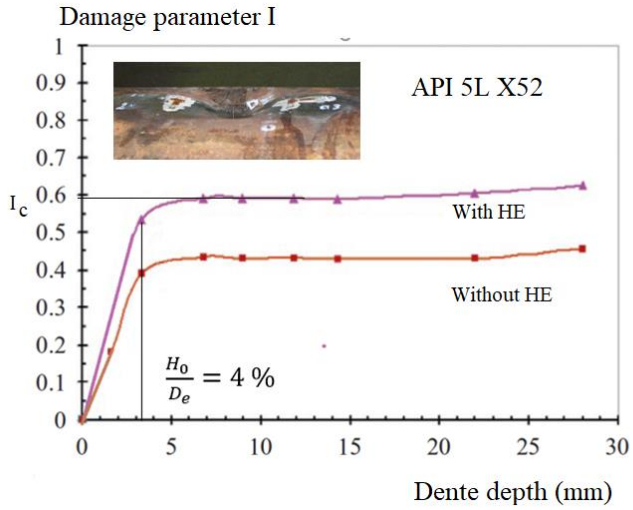


**Figure 16** Damage parameter I obtained by finite element computation (Oyane's criterion) versus dent depth [22].

### *4.4 Harmfulness of Corrosion Defect after HE*

The third reason for gas pipeline failures is external and internal corrosion defects. Figure 17 shows the typical corrosion defects on pipes made of steel.

**Figure 17** Corrosion defect in pipes made of steel [23].

The geometry of a corrosion defect is characterized by three dimensions: depth (d), length (2c), and width (2a). For conservative reasons, this type of defect is referred to as a semi-elliptical crack-like surface defect with an aspect ratio (a/c) whose value ranges from 0.1 to 1, according to the corrosion rate anisotropy in steel.

The pipe geometry and the flow stress $\sigma_0$ of the material control the failure of corrosion defects. Limit load analysis is used to determine the limit pressure for corrosion defects. The solutions for the limit pressure in pipes with corrosion defects are proposed in codes (ASME B31G [24], modified ASME B31G [25], DNV RP-F101 [26], and in the study of Choi et al. [6]). The limit pressure $p_L$ is expressed as a general equation:

$$p_L = \frac{2t}{D}.\sigma_0.\left[\frac{1-\alpha\left(\frac{a}{t}\right)}{1-\alpha\left(\frac{a}{t}\right).\frac{1}{M}}\right] \tag{19}$$

M is the Folias correction which considers the pipe curvature, and α is the geometrical parameter. Depending on the applied method, the flow stress $\sigma_0$, the geometrical parameter,α, and Folias correction M vary (see Table 7).

**Table 7** Summary of limit pressure equations.

| Method | $\sigma_0$ (MPa) | α | Folias correction M |
|---|---|---|---|
| B31G | $1.1\sigma_y$ | 2/3 | - |
| B31G | $1.1\sigma_y$ | 1.0 | ∞ |
| Modified B31G | $\sigma_y$ + 69 MPa | 0.85 | - |
| Modified B31G | $\sigma_y$ + 69 MPa | 0.85 | - |
| DNV-RP-F101 | $\sigma_{ul}$ | 1.0 | - |
| API RP-579 | $\sigma_{y/0.9}$ | 1.0 | - |

The ratio of yield stress, ultimate strength, and flow stress under $H^2$ and air are generally less than one. The difference between values under $H^2$ and air is less than 10% (Figure 18). The limit pressure is moderately impacted by HE. According to the boilermaker formula, the maximum admissible operating pressure (MAOP) is the basis for the corrosion defect evaluation in the ASME B31G code [24]:

$$\mathrm{MAOP} = \frac{\sigma_y.f_0 t}{R} \tag{20}$$

where $\sigma_y$ is the yield stress, t is the thickness, R is the radius of the pipe and $f_0$ is the design factor.

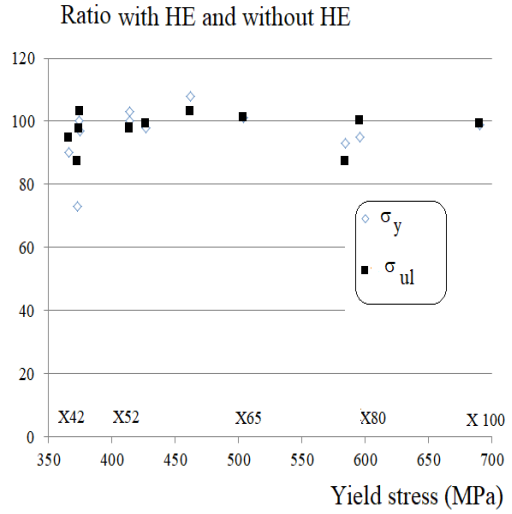


**Figure 18** The ratio of yield stress and ultimate strength with and without HE versus yield stress for 5 steel pipes (API 5L X42, X52, X65, X80, and X100)[16].

For design, the working pressure is less than the safe operating pressure $p_{safe}$. The ratio of MAOP and the safe operating pressure $p_{safe}$ is the estimated repair factor (ERF). The following condition specifies if the MAOP must be repaired or lowered:

$$\text{ERF} = \frac{\text{MAOP}}{p_{safe}} \leq 1 \text{ or } 0.95 \tag{21}$$

The defect length and the relative defect depth are represented as coordinates (2c; d/t) on a graph for this criterion. The defect assessment point is represented by the coordinates (2c*; d*/t). In the graph, the curve corresponding to the condition ERF = 1 is plotted. The defect is acceptable if the assessment point is below the assessment curve. The assessment point above the curve requires repair or working pressure de-rating. Different $p_L$ computation solutions are provided by codes (B31 or B31 mod), resulting in different assessment curves. Figure 19 presents an example of an ERF assessment diagram. The EFR assessment curve is mostly unaffected by hydrogen embrittlement.

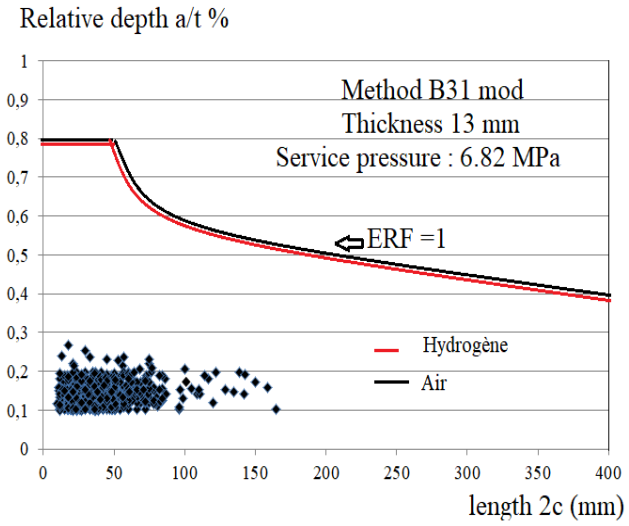


**Figure 19** Graph of a relative defect depth vs. defect length with the condition ERF = 1[16].

## 5 Lethal Risks Associated with Hydrogen

Table 1 demonstrates that hydrogen has low ignition energy, which is about 1/15 of natural gas. Although less than acetylene, hydrogen has a large flammable range in the air. Figure 20 compares the ignition energy of natural gas, propane, and gasoline vapor. Figure 21 compares the limits of flammability in the air of 16 flammable gases.

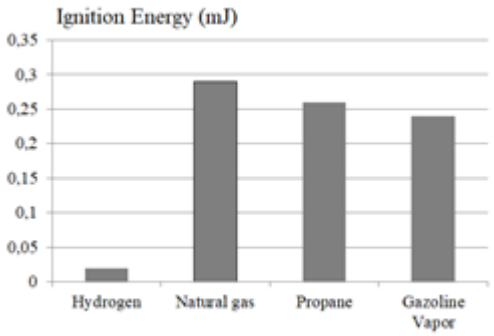


**Figure 20** Comparison of ignition energies of hydrogen, natural gas, propane, and gasoline vapor.

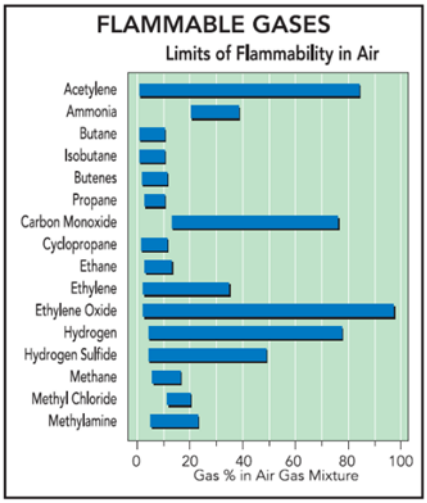


**Figure 21** Limits of flammability in the air of 16 flammable gases.

Therefore, irrespective of the ignition being immediate or delayed, hydrogen is a dangerous gas. This ignition induces torch effects or explosions, which have lethal consequences. Figure 22 shows the consequence of the explosion that occurred on Monday, June 10, 2019, at a hydrogen station in Sandvika, near Oslo, Norway.

**Figure 22** The explosion occurred on Monday, June 10$^{th,}$ 2019 at a hydrogen station in Sandvika, near Oslo, Norway.

As a result of the airbags in their cars deploying and the emergency services evacuating people in a 500 m radius quickly, the explosion caused only minor injuries to two people. Sheet metal plates were torn off and thrown onto the road and sidewalks, testifying to the blast of the explosion.

### 5.1 Immediate and Delayed Ignition

It is necessary to combine fuel and an oxidizer to provide sufficient energy for the combustion reaction to occur. An explosive atmosphere (EXAT) can be formed by mixing an oxidizer and fuel in adequate proportions. EXAT is likely to ignite in the presence of an ignition source.

Immediate ignition depends only on the characteristics of the gas (flash point, boiling temperature, flow rate, or mass of the gas released) and is completely independent of external conditions. Delayed ignition occurs a few seconds after the leak. Unlike immediate ignition, delayed ignition is governed by the characteristics of the release environment, particularly by the number and type of ignition sources present in the release's flammability zone and the effectiveness of these ignition sources.

Immediate and delayed inflammation are not independent but consecutive events, with delayed inflammation occurring only in the absence of immediate inflammation. The frequency of occurrence of a risk resulting from delayed inflammation is obtained by $(1-P_{im})$. $(P_{de})$; $P_{im}$ and $P_{de}$ are the immediate and delayed flammability probabilities, respectively. The ignition probabilities are calculated by various methods.

- The usual practice is to use databases or guides by the type of substance.
- The method of expert judgment, in which the probability is either taken as equal to 1 increasingly (any rejection ignites) or discounted by one or more factors of 10 based on an expert judgment,
- A detailed approach for which the estimation of the probability of immediate ignition is obtained according to the energy provided by the cause of the loss of confinement and the reactivity of the substance (particularly, its minimum ignition energy).
- A semi-quantitative approach was proposed earlier [20].

#### 5.1.1 Probability of Immediate Ignition

According to the standards for highly and moderately reactive gases, the gas flow Q governs the probability of immediate ignition.

- If Q < 10 kg/s, the probability of immediate ignition is 0.2.
- If the flow is between 10 and 100 kg/s, the probability of ignition is 0.5.
- If the flow is greater than 100 kg/s, the probability of ignition is 0.7.

Table 8 presents the other values proposed by INERIS [20]:

**Table 8** Probability of immediate ignition.

| | With energy source | Without energy source | |
|---|---|---|---|
| Probability of immediate ignition | 1 | 1 si Q > 10 Kg/s | 0.1 si Q < 1 Kg/s |

5.1.2 Probability of Delayed Ignition

The probabilities of delayed ignition depend on the area of risk. As presented in Table 9, these areas are classified into 4 categories.

- Zone A: Absence of sources of ignition, particularly the absence of personnel and traffic lanes, such as the zone between two production units or vertical valve discharge in the air).
- Zone B: Occasional personnel presence,
- Zone C: Heavy presence of personnel,
- Zone D: Contains possible sources of ignition, such as an external site.

**Table 9** Probability of delayed ignition.

| Zones | Zone A | Zone B | Zone C | Zone D |
|---|---|---|---|---|
| Probability of delayed ignition | 0.1 | 0.1 | 1 | 1 |

HyRAM [25] provides much lower ignition probabilities for each zone than those proposed by INERIS in Table 10. Due to the low minimum ignition energy of hydrogen, in many situations, the immediate or delayed ignition of the gas leaking from a leak orifice is assumed to be a certainty, implying that the probability of ignition is equal to one.

**Table 10** Probabilities of ignition according to HyRAM [25].

| Débit Q (Kg/s) | Immediate inflammation | Delayed inflammation |
|---|---|---|
| <0.125 | 0.008 | 0.004 |
| 0.125–6.25 | 0.053 | 0.027 |
| > 6.25 | 0.23 | 0.12 |

### *5.2. Likelihood of Lethal Damage*

At atmospheric pressure, the flammable range in the air is 4% to 75% by volume, which becomes explosive in the range of 20% to 60%. Combustion can be initiated by an extremely low-energy ignition source. A few seconds after the start of the hydrogen release, turbulent mixing between the hydrogen and the ambient air forms a cloud of inflammable gas.

Due to the nature of hydrogen gas, the cloud of flammable gas produces an explosion and has a higher burn rate than other flammable gases. A gas cloud is formed after a pipeline failure occurs. Its flow increases rapidly by the impulse of the vented gas, and a quasi-steady gas jet is established. A blazing flare is produced if the released gas ignites immediately after the failure. A significant explosion occurs if the gas cloud is subjected to delayed ignition.

The prominent lethal risks can be the consequence of overpressure or the thermal effect of radiation caused by a sustained fire, which can be preceded by an explosion. An explosion model of the gas cloud that characterizes the overpressure and a fire model that provides the intensity of the heat can be used to estimate the surface of the ground affected by a pipeline failure. The gas release rate (Q) of a failure is associated with the magnitude of the explosion and the corresponding size of the danger zone. The rate of hydrogen release depends on the service pressure of the pipeline, the length of the pipeline, and the effective size of the hole. The diameter

of the pipe, the operating pressure, and the length of the pipeline from the point of supply to the point of failure determine the parameters of the danger zone when the effective size of the hole is large, i.e., greater than the diameter of the pipeline. As shown in Figure 16, the size of the danger zone depends on the pipe dimensions, operating pressures, and pipeline length.

The probability of lethal damage is linked to the probability of the presence of a person near the failure zone of the pipe. Given the difficulty of establishing this probability of presence, it is preferable to reduce or increase the probability of risk by a coefficient, $C_{ev}$, which depends on the environment (Table 11).

**Table 11** Values of the $C_{ev}$ coefficient according to the location.

| Location | $C_{ev}$ | Environment | $C_{ev}$ |
|---|---|---|---|
| Country | 0.8 | Urban zone | 3 |
| Parking | 1 | Industrial zone | 0.05 |

### *5.3 Probability of Lethal Heat Damage*

The level of lethal heat radiation damage depends on both the intensity of the heat flux and the duration of the exposure. At a specified location of interest, the thermal dosage unit (V) combines the radiant heat flux I in W/m2 and the exposure time t in seconds:

$$\mathrm{V} = \mathrm{I}^{(4/3)}\mathrm{t} \tag{22}$$

The probability of death $P_{dec}$ is a function of heat flux intensity s, which is estimated by Eq. 23 [20]:

$$P_{dec} = \frac{1}{\sqrt{2\pi}} \int_{-\infty}^{P_{ro}} e^{-s^2/2}\, ds \tag{23}$$

The value of the probit $P_{ro}$ is expressed in [24]:

$$P_{ro} = -14.9 + 2.56Ln\left(\frac{I^{(4/3)}t}{10^4}\right) \tag{24}$$

The heat flow is impacted by the shape of the flame at a particular distance from a jet fire. A flaming torch is considered a series of point heat emitters. The radiation received from each emitter and point source is added to obtain the total heat flux reaching a given point. According to API RP 521 [25], the heat flux at some distance from the fire source is calculated:

$$I = \frac{\pi \tau_a Q_{ef} H_c}{4\pi r^2} \tag{25}$$

where $\tau_a$ denotes the atmospheric transmissivity, $Q_{ef}$ denotes the effective rate of gassing, $H_c$ denotes the heat of combustion ($H_c$ = 1.419 × 108 J/kg), and r denotes the radial distance between the fire and the area of interest.

$$Q_{ef} = 6.47.10^{-4} A_p \alpha p_s * max\left[0.3; \frac{1}{\sqrt{1 + A_p}}\right] \quad (26)$$

where a represents the size of the dimensionless hole, $p_s$ represents the working pressure, $A_p$ represents the cross-section of the pipe, and L represents the length of the pipe from the gas supply station to the point of ignition of the fire. The unit of probability or probit $P_{ro}$ is expressed as follows [6]:

$$P_{ro} = a + b \ln D \quad (27)$$

where a and b are the empirical constants of the dose-effect relationship. The atmospheric transmissivity $\tau_a$ is conservatively assumed to be equal to unity ( $\tau_a$ = 1). Therefore, the probit equation can be written as follows:

$$P_{ro} = -19.18 + 3.4Ln\left(\frac{Q_{ef}}{r^2}\right) \quad (28)$$

The heat of combustion of hydrogen gas at room temperature is the basis of Eq. 28. We consider a threshold thermal intensity level that is associated with 1% death for those exposed for 30 s before finding a shelter. The thermal intensity threshold to compute the size of the danger zone by thermal radiation is assumed to be 15 kW/m2. Putting Eq. (28) into Eq. (23) gives the radial distance from the failure point to the location where the heat flux is equal to the threshold value of 15 kW/m2.

$$r_{feu} = 0.24D\sqrt{\alpha p_0} * \sqrt{max\left[0.3; \frac{1}{\sqrt{1 +}}\right]} \quad (29)$$

### *5.4 Probability of Lethal Damage Due to Explosion Overpressure*

It is assumed that a hydrogen explosion is equivalent to a TNT explosion with the same energy. The overpressure caused by the explosion is estimated as a function of distance from its equivalent mass of TNT. The equivalent mass of TNT is computed from the heat of combustion of hydrogen, the total mass of hydrogen released, the explosion efficiency, and the explosion energy of TNT. A typical value for the energy of the explosion of TNT is 4686 kJ kg. The explosion efficiency of a hydrogen vapor cloud is 0.03. Therefore, the maximum equivalent mass of TNT $m_{TNT}$ is estimated as:

$$m_{TNT} = 0.03.75\pi d^2 \alpha \sqrt{\gamma \rho_0 p_0 \left[\frac{2}{(\gamma + 1)}\right]^{(\gamma+1)/\gamma-1}} \quad (30)$$

Here, D is the pipe diameter, $\alpha$ is the dimensionless hole size, and $p_0$ is the pressure at operating conditions. The maximum equivalent mass in TNT is:

$$m_{TNT} = 4.57.10^{-3} d^2 \alpha p_0 \quad (31)$$

The explosion pressure generated is given as:

$$\frac{p_e}{p_{ea}} = \frac{1616[1 + (z_e/4.5)^2]}{\sqrt{[1 + (z_e/0.048)^2]}[1 + (z_e/0.32)^2][1 + (z_e/1.35)^2]} \tag{32}$$

$$z_e = \frac{r}{0.166(D^2 \alpha p_0)^{1/3}} D^2 \alpha p_0 \tag{33}$$

Here, r is the distance. Figure 23 displays an example of the explosion area.

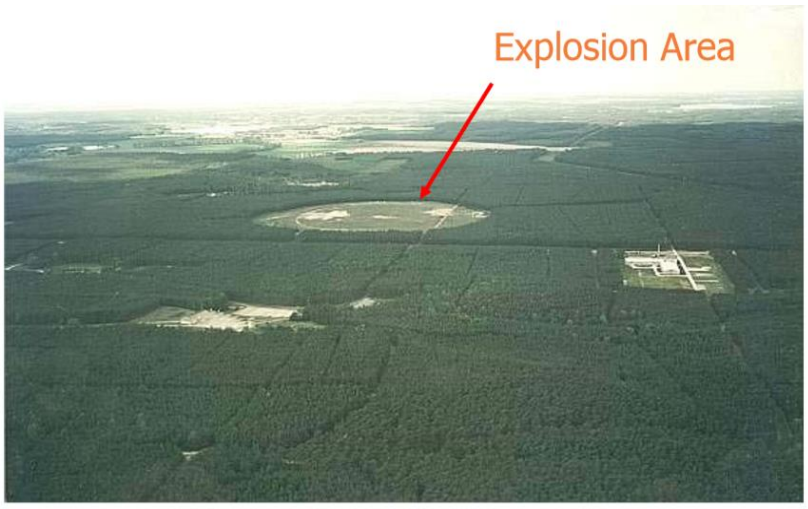


**Figure 23** Hydrogen explosion area [6].

The death probability $P_{dec}$ is estimated by Eq. 34:

$$P_{dec} = \frac{1}{\sqrt{2\pi}} \int_{-\infty}^{P_{ro}} e^{-s^2/2}\, ds \tag{34}$$

With s, the $m_{TNT}$. The probit function [26] is:

$$P_{ro} = -77.1 + 6.91 Ln(p_e) \tag{35}$$

The level of overpressure threshold f associated with 1% death in exposed individuals is 21.3 KPa [6].

The radius of a circular zone surrounding the assumed point of failure for which exposure to overpressure caused by an explosion has a 1% probability of causing death is estimated by Eq. 36. The maximum danger distance $r_{expl}$ (measured in meters) increases with the service pressure of the pipeline. This distance corresponds to the overpressure threshold of 21.3 KPa. Figure 24 shows the distances $r_{expl}$ plotted against the service pressure.

$$\mathrm{r_{expl}} = 1.58\alpha^{1/3}\mathrm{d}^{2/3}\mathrm{p_0}^{1/3} \tag{36}$$

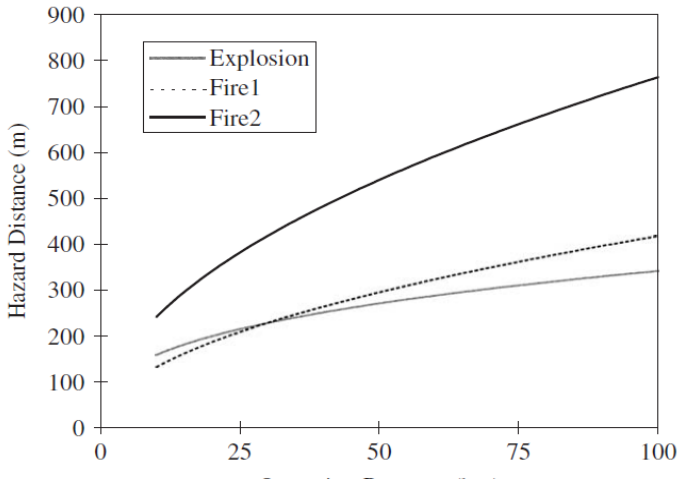


**Figure 24** The maximum danger distance increases according to the service pressure of the pipeline (diameter D = 1 m) [26]. Explosion: distance corresponding to 21.3 KPa; Fire 1: distance corresponding to 15 kW/m2 with decay factor assumed to be equal to 0.3; Fire 2: distance corresponding to 15 kW/m2 with decay factor assumed to be equal to 1) [26].

The values of the dangerous distance per explosion in the case of a hydrogen-natural gas mixture were determined by NATURALHY [6] using a risk assessment model. Figure 25 shows an example of a pipe with a 914 mm diameter and a service pressure of 70 bars. The risk drops to zero just over 400 m from the pipe failure. This distance is decreased by about 25 m by adding 25% hydrogen. The dangerous distance is reduced by about 75 m and 100 m for 50% and 75% mixtures, respectively. According to this result, site-specific risks vary depending on the population density near the pipeline [27].

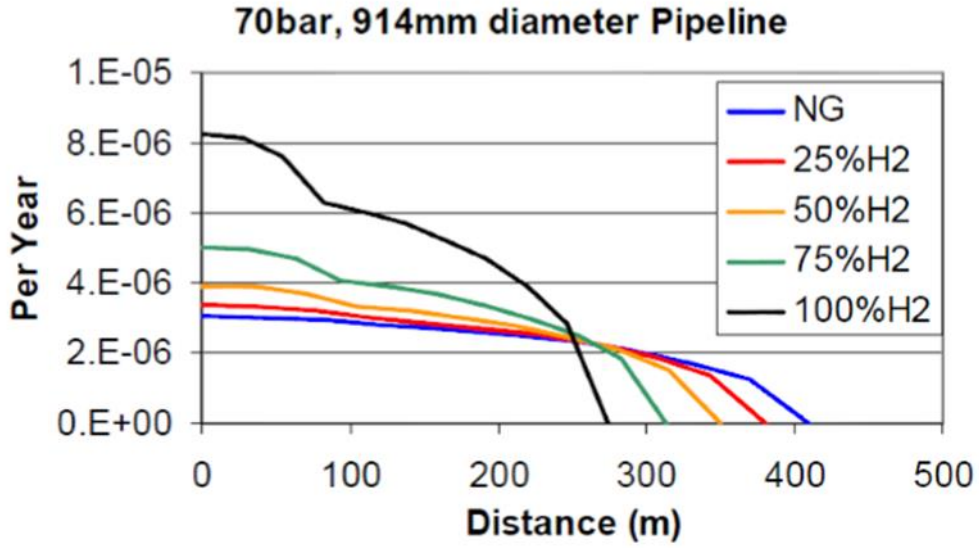


**Figure 25** The risk of death per year per individual depending on the distance from the pipe leak [6].

### *5.5 Lethal Effects and Probabilistic Design Factor*

The risk equation can be written as follows:

$$P_r(Risk) = P_r(L) * P_r(Q) * P_r(I) * P_r(LE) * P_r(pers) * L * C_{ev} * C_{rr} \quad (37)$$

- $P_r$ (L) is the probability of leakage after failure,
- $P_r$ (Q) is the probability of having a gas flow lower than a prescribed value,
- $P_r$ (I) is the probability of ignition,
- $P_r$ (LE) is the probability of lethal effects greater than a threshold value,
- $P_r$ (pers) is the probability of the presence of a person,
- L is the length of the pipeline considered,
- $C_{ev}$ is the coefficient considering the location of the pipeline,
- $C_{rr}$ is the risk reduction factor considering the risk reduction measures.

Expert judgments provide the values of $P_r$ (I), $P_r$ (LE), and $P_r$ (pers). The calculations enable the determination of the values of the probability of leakage $P_r$ (L) and the probability of having a gas flow lower than a prescribed value Pr (Q). $C_{ev}$ and $C_{rr}$ are given by codes. Table 12 shows the minimum, maximum, and chosen values of these parameters. The choice is justified by conservatism in risk assessments. When the service pressure $p_s$ exceeds the maximum admissible operating pressure (MAOP), the leak probability is calculated as:

$$P_s \geq MAOP \quad (38)$$

**Table 12** Minimum, maximum, and chosen values for $C_{ev}$, $C_{rr}$, Pr (I), Pr (Q), Pr (EF).

| Terme | Mini | Maxi | Choix | Justification of choice |
|---|---|---|---|---|
| $C_{ev}$ | 0.8 | 3 | 0.8–3 | Depending on the environment rural, peri-urban or urban areas |
| $C_{rr}$ | 0.01 | 1 | 1 | No specific protection |
| Pr (Q) | 0.2 | 0.5 | 0.5 | 0.5 corresponds to a flow ranging from 10 to 100 kg.s$^{-1}$ (computed flow rate is 16 kg.s$^{-1}$) |
| Pr (I) | 0.04 | 0.5 | 0.5 | 0.5 corresponds to the probability of immediate inflammation |
| Pr (EF) | 0 | 0.04 | 0.04 | The probability of 0.04 is associated with lethal risk caused by the thermal effect<br>0 corresponds to the lethal risk emanating from the overpressure effect. |

The yield stress $\sigma_y$, the thickness t, and the radius of the pipe R are considered stochastic. Eq. 20 enables the computation of the stochastic maximum admissible operating pressure with parameters given in Table 13.

**Table 13** Distribution parameters and distribution law associated with each input variable.

| Variable | Mean μ | Standard Deviation | Skewness | Kurtosis | Distribution law |
|---|---|---|---|---|---|
| Yield stress | 515.4 MPa | 28.89 MPa | -0.007 | 3.00 | Normal |
| Thickness | 5.2 mm | 0.24 mm | -0.0029 | 2.99 | Normal |
| Diameter | 314 mm | 0.79 mm | -0.00076 | 3.00 | Normal |
| MAOP | 17.07 MPa | 1.24 MPa | 0.10 | 3.01 | Normal |

Eq. 37 is computed for the 3 locations (rural, peri-urban, and urban areas). Table 14 presents the values of each component of this equation. As an excellent compromise between safety and cost, the conventional probability of risk of $10^{-5}$ is generally accepted by pipe codes. Table 14 reports the probability of leak $P_r$ (L), the values of MAOP, and the probabilistic design factor $f_{0,\mathrm{prob}}$ for the three locations.

**Table 14** Summary of the parameter values of Eq. 37 for the 3 locations.

| Location | Rural area | Peri-urban area | Urban area |
|---|---|---|---|
| $P_r$ (Risk) | 0.00001 | | |
| L (km) | 100 | | |
| $C_{rr}$ | 1 | | |
| $P_r$ (Q) | 0.5 | | |
| $P_r$ (I) | 0.5 | | |
| $P_r$ (EF) | 0.04 | | |
| $P_r$ (Pers) | 0.1 | 0.5 | 1 |
| $C_{ev}$ | 0.8 | 3 | 3 |
| $P_r$ (L) | $1.25.10^{-4}$ | $6.67.10^{-6}$ | $3.33.10^{-6}$ |
| MAOP (MPa) | 12.5 | 11.7 | 11.5 |
| $f_{0,\mathrm{prob}}$ | 0.8 | 0.7 | 0.7 |

Table 15 provides a comparison between the probabilistic design factor $f_{0,\ prob}$, and the deterministic one $f_{0,\ det,}$ given by [1]. The deterministic values are more conservative. In [10], since there is no information on how these values were obtained, it is assumed that they were obtained by expert judgment.

**Table 15** Values of design factors $f_{0,\ prob}$, and $f_{0,\ det}$ according to locations.

| | Rural area | Peri-urban area | Urban area |
|---|---|---|---|
| $f_{0,\mathrm{prob}}$ | 0.8 | 0.7 | 0.7 |
| $f_{0,\mathrm{det}}$ | 0.6 | 0.5 | 0.4 |

MAOP is computed from the yield stress, a material parameter that suffers from some scatter. This scatter is measured by the coefficient of variation, COV. Table 16 shows the influence of the

yield stress COV on the probabilistic design factor. If COV varies in the range [0.05–0.20] for an urban area, the MAOP decreases by 90% and the design factor by 85%.

**Table 16** Influence of COV of yield stress on MAOP based on location.

| Location | COV | MAOP (MPa) | $f_{0,prob}$ |
|---|---|---|---|
| Rural area | 0.05 | 13.7 | 0.8 |
| Peri-urban area | | 12.9 | 0.7 |
| Urban area | | 12.8 | 0.7 |
| Rural area | 0.1 | 10.7 | 0.6 |
| Peri-urban area | | 9.4 | 0.5 |
| Rural area | | 9.1 | 0.5 |
| Country area | 0.15 | 7.7 | 0.4 |
| Peri-urban area | | 5.7 | 0.3 |
| Urban area | | 5.3 | 0.3 |
| Rural area | 0.2 | 4.5 | 0.2 |
| Peri-urban area | | 1.9 | 0.1 |
| Urban area | | 1.4 | 0.1 |

A design factor greater than 0.5 A is guaranteed if the COV is less than 0.1. This low COV value is obtained in modern steel. Vintage steels have a higher COV. An economical threshold gas flow is one with an MAOP value of 50 MPa (MAOP* in Figure 25). Therefore, one cannot tolerate in the pipe networks some parts with vintage steel exhibiting a COV greater than 0.15 (Figure 26).

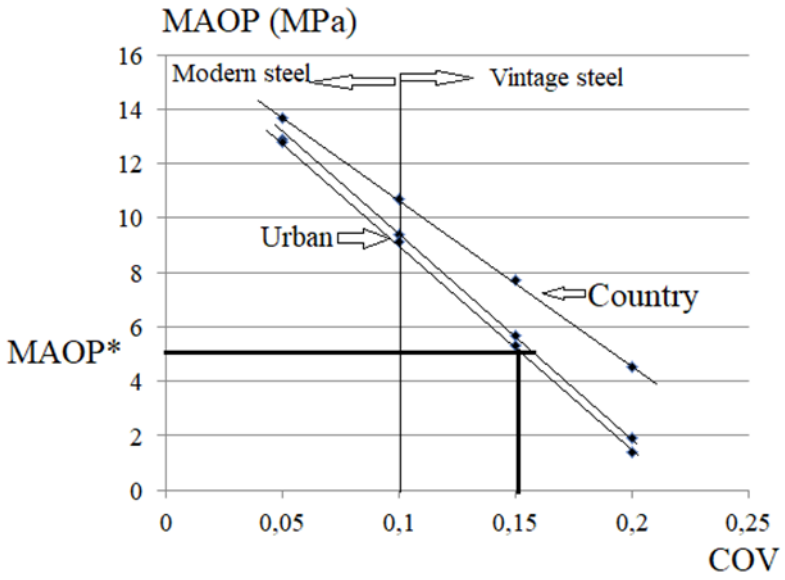


**Figure 26** MAOP versus COV of yield stress on MAOP for urban, peri-urban, and country locations [13].

### *5.6 Hydrogen Loss in Polyethylene Pipes Due to Permeation*

Due to the small size of hydrogen molecules, the diffusion of molecular hydrogen through polymeric materials is relatively rapid. Hydrogen can slowly seep through the pipe walls and be

trapped in closed spaces [28]. This is a huge risk for insulated and/or buried tubes, as well as for tubes in closed rooms and cupboards where hydrogen can accumulate. The accumulated hydrogen then ignites or even explodes at a later stage.

A transmission pipe in HDPE with an outer diameter of 110 mm and a wall thickness of 10 mm, filled with hydrogen at 10 bars, has a permeation rate for one kilometer of 70 liters per 24 h.

This permeation rate increases with hydrogen pressure and decreases with the wall thickness. For natural gas, the flow is 10 to 50 times lower than that for hydrogen.

Furthermore, sealing polymer pipes is a challenging issue. The connections between the different pipes will need to be better connected than those conventionally used for natural gas. Otherwise, hydrogen will escape through the seal, the risk of which strongly depends on the possibility of hydrogen accumulating in the surrounding space.

The concentration on the contact surface is unknown during gas diffusion. However, the vapor pressure of the gas is known. According to Henry's law, the concentration of gas is proportional to the pressure of that gas. Therefore, for an isothermal system, the concentration of gas at the surface of the polymer is given by:

$$C_H = S * p_H \tag{39}$$

where S is the gas solubility (mol/Pa.cm$^2$), $C_H$ is the hydrogen concentration (mol/cm$^3$), and $p_H$ is the gas pressure (Pa). Assuming that diffusion is independent of pressure, Fick's first law for diffusion is utilized to determine permeability ($P_e$). It is defined as:

$$P_e = DS \tag{40}$$

where D is the diffusion coefficient (cm$^2$/s). The two methods to determine the permeability or permeation parameters are the steady-state method and the transient method. The steady-state method is based on the flow information when the gas concentration is constant at all points in the polymer. The transient method is based on the permeation history from the beginning of the diffusion until the end of the process or until the state of equilibrium is attained.

The permeability of polyethylene PE80 in the presence of methane and hydrogen was determined [6] for three temperatures. Table 17 presents the results.

**Table 17** Permeability of polyethylene PE80 in the presence of methane and hydrogen determined for three temperatures [6].

| Polymère | Température°C | Pe (Méthane) cm$^3$.cm/cm$^2$.s.bar | Pe (hydrogène) cm$^3$.cm/cm$^2$.s.bar |
|---|---|---|---|
| PE 80 | 80 | $11.5 \times 10^{-8}$ | $24.1 \times 10^{-8}$ |
| PE 80 | 60 | $4.33 \times 10^{-8}$ | $11.8 \times 10^{-8}$ |
| PE 80 | 40 | $1.14 \times 10^{-8}$ | $4.80 \times 10^{-8}$ |

In the NATURALHY contract [6], the permeation loss of plastic pipes has been investigated. In this paper, actual pipes and assemblies were tested at operating temperatures and pressures with a mixture of hydrogen and methane.

In this paper, three different types of PE (PE 63, PE80, and PE100) with diameters ranging from 20 mm to 200 mm are subjected to pressures between 1 bar and 12 bar and temperatures between 5°C and 25°C. Table 18 shows the permeation coefficients of methane and the methane plus hydrogen mixture for pressures of 4, 8, and 12 bars in a PE80 pipe with a diameter of 32 mm.

**Table 18** Permeability of polyethylene PE 80 in the presence of methane and hydrogen and loss of hydrogen (NATURALHY contract [6]).

| Gas | Pressure (Bars) | Pe $cm^3.cm/cm^2.s.bar$ | loss $H^2$ l/Km/year |
|---|---|---|---|
| CH4 | 4 | $11.8 \times 10^{-8}$ | NA |
| 90% CH4 + 10%H2 | 4 | $9.1 \times 10^{-8}$ | 186,3 |
| 90% CH4 + 10%H2 | 8 | $10.8 \times 10^{-8}$ | 546,3 |
| 90% CH4 + 10%H2 | 12 | 10.8 | 854,3 |

Furthermore, Table 18 presents the calculated gas loss. The incubation time for hydrogen is nearly zero, which is considerably higher than the incubation time for methane. In the hydrogen/methane mixture, the permeation coefficient of hydrogen is four to five times higher than that of methane and increases with internal pressure. The permeation coefficient significantly changes as PE ages. However, the aging of the pipes has no significant influence on the permeation coefficients. In the NATURALHY contract [6], typical values of hydrogen leak rate from PE and PVC pipes were computed for

- PVC-CPE delivering pure H2: 5.0 liters/km/day.
- PVC with the same internal pressure as pure H2: 13.2 liters/km/day.
- PE under 4 bars of internal pressure with 80% natural gas and 20% hydrogen: methane-0.7 liter/km/day and hydrogen-2.3 liters/km/day.

## 6. Conclusion

Numerous papers focus on the promotion of hydrogen as a sustainable energy carrier and a source of energy. However, these papers seldom discuss the risks associated with the use of this gas. Hydrogen is a dangerous gas for the following reasons:

i) It has low ignition energy.
ii) A wide flammability range.
iii) It promotes the embrittlement of steel.
iv) Hydrogen loss via polymer pipes is crucial due to a high permeation coefficient, particularly when it accumulates in the surrounding space.

Therefore, it is necessary to consider the risks while designing and implementing maintenance and surveillance operations for the transport of hydrogen via pipes.

The failure assessment diagram must be used to compute the safety factor to determine the cruciality of the pipes. The consequences of the decrease in the safety factor following hydrogen embrittlement include derating MAOP or lowering service pressure. The significant drop in failure elongation after HE is taken into consideration when calculating the damage associated with large deformation defects such as dents or ovalization.

The lethal risks from the torch effect or explosion are considered while modifying the design factor in the calculation of the MAOP depending on the location of the pipes.

Leaks due to hydrogen permeation through domestic hydrogen distribution networks must be monitored, particularly in closed areas. Furthermore, the generalization of the domestic use of hydrogen must be the subject of new regulations.

## Author Contributions

Project development: P.G; C.J. Data collection: P.G; C.J. Writing: P.G; C.J.

## Competing Interests

The authors have declared that no competing interests exist.

## References

1. Quincy MA. NFPA 704: Standard system for the identification of the hazards of materials for emergency response. NFPA. 2006. doi:10.13140/RG.2.2.32358.01608.
2. Thompson AW, Bernstein IM. Stress corrosion cracking and hydrogen embrittlement. In: Metallurgical treatises. Metallurgical Society of AIME; 1983. Available from: https://inis.iaea.org/search/search.aspx?orig_q=RN:16029970.
3. Oriana RA. The physical and metallurgical aspects of hydrogen in metals. Fusion Technol. 1994; 26: 235-266.
4. Steigerwald EA, Schaller FW, Troiano AR. The role of stress in hydrogen induced delayed failure. Trans Met Soc AIME. 1960; 218: 832.
5. Magnin T. Mécanismes de fatigue-corrosion des alliages métalliques. Revue de Métallurgie. 2002. doi:10.1051/metal:2002161.
6. Florrisson O. Preparing for the hydrogen economy by using the existing natural gas system as catalyst (NATURALHY). European Commission; 2010; SES6/CT/2004/502661.
7. Capelle J, Dmytrakh I, Pluvinage G. Electrochemical hydrogen absorption of API X52 steel and its effect on local fracture emanating from notches. Struct Integr Life. 2009; 9: 3-8.
8. Osage DA, Janelle JL. Fitness-for-service, API 579-1/ASME FFS-1. Proceeding of ASME 2008 Pressure Vessels and Piping Conference. 2008 July 27-31; API and ASME. DOI: 10.1115/PVP2008-61796.
9. Hydrogen piping and pipelines. ASME; 2020; B31.12-2019. Available from: https://www.asme.org/codes-standards/find-codes-standards/b31-12-hydrogen-piping-pipelines.
10. Coseru A, Capelle J, Pluvinage G. On the use of Charpy transition temperature as reference temperature for the choice of a pipe steel. Eng Failure Anal. 2014; 37: 110-119.
11. Oldfield W. Development of fracture toughness reference curves. J Eng Mater Technol. 1980; 102: 107-117.
12. Kpemou AM, Guy P, Julien C. Influence of hydrogen embrittlement on ductile-brittle transition temperature determined on mini-charpy specimens made in x65 steel. J Fail Anal Prev. 2021; 21: 2290-2304.

13. Mijim JK, Pluvinage G, Capelle J, Azari Z, Benamara M. Probabilistic design factors for pipes used for hydrogen transport. Int J Hydrogen Energy. 2020; 45: 33860-33870.
14. 6th Report of the European Gas Pipeline Incident Data Group, 1970-2004. EGIG; 2005. Available from: https://www.egig.eu/reports/$60/$66.
15. Pluvinage G. Notch effects in fatigue and fracture. In: Notch effects in fatigue and fracture. Dordrecht: Springer; 2001. pp.1-22.
16. Guy P, Laszlo T, Julien C. Effects of hydrogen addition on design, maintenance and surveillance of gas networks. Processes. 2021; 9: 1219.
17. Bouledroua O, Hadj Meliani M, Pluvinage G. Assessment of pipe defects using a constraint-modified failure assessment diagram. J Fail Anal Prev. 2017; 17: 144-153.
18. Akourri O, Louah M, Kifani A, Gilgert G, Pluvinage G. The effect of notch radius on fracture toughness $J_{Ic}$. Engineering Fracture Mechanics. 2000; 65: 491-505.
19. Razpoko N. A comparison of experimental results and computations for cracked tubes subjected to internal pressure. Mater Tehnol. 2006; 40: 233.
20. INERIS DRA 71-Opération B, Proposition d'une méthode semi-quantitative d'évaluation des probabilités d'inflammation. INERIS; 2015; N° DRA-13-133211-12545A. Available from: https://www.ineris.fr/sites/ineris.fr/files/contribution/Documents/dra-13-133211-12545a-evaluation-des-proba-dinflammation-v8-1442302458.pdf.
21. Groth KM, Hecht ES. HyRAM: A methodology and toolkit for quantitative risk assessment of hydrogen systems. Int J Hydrogen Energy. 2017; 42: 7485-7493.
22. Allouti M, Schmitt C, Pluvinage G, Gilgert J, Hariri S. Study of the influence of dent depth on the critical pressure of pipeline. Eng Fail Anal. 2012; 21: 40-51.
23. Pluvinage G, Bouledroua O, Meliani MH, Suleiman R. Corrosion defect analysis using domain failure assessment diagram. Int J Pres Ves Pip. 2018; 165: 126-134.
24. Jo YD, Ahn BJ. Analysis of hazard area associated with hydrogen gas transmission pipelines. Int J Hydrogen Energy. 2006; 31: 2122-2130.
25. Guide for pressure-relieving and depressuring systems. Washington, DC: API; 1990. Available from: https://standards.globalspec.com/std/725643/api-rp-521.
26. Jo YD, Ahn BJ. A simple model for the release rate of hazardous gas from a hole on high-pressure pipelines. J Hazard Mater. 2003; 97: 31-46.
27. Melaina MW, Antonia O, Penev M. Blending hydrogen into natural gas pipeline networks: A review of key issues. National Renewable Energy Laboratory; 2013.
28. Foulc MP, Nony F, Mazabraud P, Berne P, Klopffer MH, Flaconneche B, et al. Durability and transport properties of polyethylene pipes for distributing mixtures of hydrogen and natural gas. Proceedings of the 16th World Hydrogen Energy Conference; 2006 June 13-16; Lyon, France. Association Francaise pour l'Hydrogene et les Piles a Combustible (AFHYPAC).


Enjoy *JEPT* by:

1. Submitting a manuscript
2. Joining in volunteer reviewer bank
3. Joining Editorial Board
4. Guest editing a special issue

For more details, please visit:
http://www.lidsen.com/journal/jept